

We are IntechOpen, the world's leading publisher of Open Access books Built by scientists, for scientists

6,900

Open access books available

185,000

International authors and editors

200M

Downloads

Our authors are among the

154

Countries delivered to

TOP 1%

most cited scientists

12.2%

Contributors from top 500 universities



WEB OF SCIENCE™

Selection of our books indexed in the Book Citation Index
in Web of Science™ Core Collection (BKCI)

Interested in publishing with us?
Contact book.department@intechopen.com

Numbers displayed above are based on latest data collected.
For more information visit www.intechopen.com



The Synergy of Electrochemistry and Concrete Material Science in Evaluating Corrosion Resistance of Wastes-Containing Reinforced Cement-Based Systems

D. A. Koleva and K. van Breugel

*Delft University of Technology, Faculty of Civil Engineering and Geosciences,
Department Materials & Environment, Stevinweg 1, 2628CN Delft,
Netherlands*

1. Introduction

Next to water, concrete is the most used material on earth. Reinforced concrete has the potential to be durable and capable of withstanding a variety of adverse environmental conditions. One of the major difficulties in the engineering practice, however, is the multi-dimensional nature of reinforcement corrosion related issues. Nevertheless, materials and processes involved in the service life of a civil structure and their interaction are independently weighed and are seldom brought together. Very often the design of concrete mix proportions and the design of protective measures (such as the application of coatings or electrochemical techniques) are made in separate steps and (positive or negative) interactions among themselves are neglected. The most original aspect of this work is the integration of fundamental electrochemical techniques and concrete material science within monitoring and assessment of the corrosion performance of reinforced cement-based materials. Further, hereby discussed is the implementation of an eco-friendly approach of waste utilization for corrosion control and/or achieving superior properties and performance.

Reinforced cement-based systems (e.g. reinforced mortar and concrete) are multi-phase composite materials at different levels of aggregation. Hence, multi-phase interfaces are involved in their structural performance and material behaviour. The steel reinforcement is embedded (on meso-level, generally relevant to mm dimension) in supposedly homogeneous cement-based bulk matrix. However, on a lower structural level (micro-level, expressed in μm), the bulk material consists of cement paste and aggregate particles, with air voids and macro pores dispersed in the cement paste matrix. Further, the cement paste can be decomposed into un-hydrated cement, hydration products, and capillary pore structure. The latter is generally assumed to have significant relevance to permeability and other transport phenomena in concrete technology.

Both the reinforcement corrosion processes (i.e. electrochemical phenomena) and the development of the cement-based microstructure are influencing the material structure in reinforced cement-based materials (as mortar or concrete) on macro and micro/nano level. The corrosion process on one hand and hydration mechanisms on the other, determine changes in microstructural properties and ion transport, compared to rest conditions (in

non-corroding systems). Chloride penetration and further corrosion will induce structural alterations of the composite material in various aspects, e.g. modifying the pore structure and interfacial zones, inducing cracking at the steel–paste interface (as a result of volume expansion of corrosion products) and further crack propagation in the bulk matrix. These microstructure alterations are underlying the evolution of electrical behaviour of reinforced mortar (concrete) during the corrosion process (as previously investigated by the authors (Koleva et al., 2008) unfavourable pore structure alterations in cement-based materials yield non-uniform electrical properties and thereby possibly result in disturbance of the electrolytic path due to heterogeneities and instabilities inherent to the bulk matrix). The electrical properties and the material microstructure undergo continuous changes due to complicated cement hydration and steel corrosion process. The correlation of electrical properties, pore solution chemistry, local microstructure of the material (in terms of porosity, pore size distribution, pore connectivity, etc.) logically influence the corrosion resistance and electrochemical behaviour of the embedded steel reinforcement. Whereas the bulk matrix properties are generally separately evaluated via well known methods and techniques of concrete material science, the reinforcement behaviour is mostly considered separately as well, using the means of electrochemical and corrosion science. However, if a reinforced cement-based system (heterogeneous and non uniform at different levels) has to be evaluated in terms of corrosion resistance and therefore service life performance, a thorough and reliable investigation and recommendation is only possible if considering the integration of both concrete material science and electrochemistry.

In the framework of an extensive experimental study on corrosion, electrochemical protection (cathodic protection efficiencies) and novel approaches for corrosion control (employment of tailored nano-aggregates and wastes) the authors have investigated the electrochemical phenomena of steel reinforcement corrosion in aggressive environments by means of electrochemical techniques, e.g. Electrochemical Impedance Spectroscopy (EIS), Potentiodynamic polarization (PD), Cyclic voltammetry (CVA). Microscopic and image analysis techniques (e.g. Scanning electron microscopy (SEM) and Energy dispersive X-ray (EDX)) render possible quantitative characterization of the composite microstructure at various interfaces, including structural morphology of steel corrosion and cement hydration products, pore structure, as well as the interfacial transition zones between cement paste and aggregate or bulk cementitious matrix and steel. Steel surface properties for all investigated cases were (as generally) determined via X-ray analysis (X-ray diffraction (XRD) and X-ray photoelectron spectroscopy (XPS)).

This chapter will discuss and give examples for the integration of electrochemical methods and microstructural investigation in reinforced cement-based materials within conditions of chloride-induced corrosion. Further, the chapter will discuss an eco-friendly approach to corrosion control in reinforced cement-based systems, by involving waste utilization (slag, from the steel production and red mud, from the aluminum production), presenting material properties and materials interactions in the context of improved long-term service life in civil engineering applications.

2. OPC and BFS cement concrete: Correlation of electrochemical parameters and microstructural characteristics

This paragraph reports on the electrochemical behavior of construction steel (FeB500 HKM), correlated with microstructural characterization of the bulk matrix in reinforced concrete,

using Ordinary Portland cement (OPC), CEM I and Blast Furnace Slag (BFS) cement, CEM III/B. The corrosion initiating environment was 5% NaCl. Potential mapping, Electrochemical Impedance Spectroscopy (EIS) and Potentio-dynamic polarization (PDP) were employed to evaluate the corrosion performance of the embedded steel. The electrochemical parameters were further coupled with pore structure parameters, thus establishing the reason for the postulated higher corrosion resistance of reinforcing steel in BFS reinforced concrete.

Concrete (reinforced concrete respectively), using BFS cement, is widely used in practical applications in Northern European countries (Çopuroğlu O. et al. 2006b). Since BFS is a by product (within the process of steel production), it can be considered as an ecologically friendly manner of minimizing the usage of cement and CO₂ emissions respectively. From the view point of bulk cement matrix characteristics, a wide range of investigations are reported, discussing cementitious materials with BFS cement (Çopuroğlu O. et al. 2006b, Bouikni A. et al. 2009, Dehghanian C. et al. 1997, Thomas M. D. A. et al. 1999, Audenaert K., et al. 2010, Li S. et al. 1986). Steel behaviour in BFS concrete is also reported, although not as widely investigated, as the bulk cementitious matrix only (Dehghanian C. et al. 1997, Song Ha-Won, et al. 2006, Pal S.C., et al. 2002, Dinakar P., et al. 2007, Macphee D.E., et al. 1993, Baweja D., et al. 1998). Compared to OPC concrete, the major contribution of BFS has been identified to result in a denser pore structure (Bouikni A. et al. 2009, Giorv O. E., et al. 1979, Manmohan D., et al. 1981, Kumar A.D.M. 1986, Hooton R.D., 1986) and reduced global porosity (Copuroglu O., 2006a). These considerations are directly linked to eventual beneficial influence of BFS, related to chloride-induced steel corrosion in reinforced concrete. Studies have shown that the use of BFS may reduce the probability of steel corrosion due to decreased permeability (Ramezani pour A.A., 1995, Osborne G.J., 1999, Irassar E. F., et al. 2000, Hossain K. M. A., et al. 2004, Gjorv O. E. 1995), low electrical conductivity and refined pore structure (Song Ha-Won, et al. 2006, Efes Y. 1980, Dehghanian C. 1999, Gu P., et al. 2000). Other studies, however, either report close and significant dependence of the corrosion rate on the BFS content [Song Ha-Won, et al. 2006, Pal S.C., et al. 2002], or report on decreased corrosion resistance in BFS concrete at early hydration stages (Song Ha-Won, et al. 2006) and higher corrosion rates in BFS due to limited oxygen availability and thus shift of the corrosion potential of the steel surface to a more negative (active) state (Dehghanian C. et al. 1997). To this end this paragraph aims to illustrate that a thorough evaluation of the reinforced concrete system (in this case when BFS is involved in comparison to ordinary OPC concrete), is only possible via the synergy of electrochemistry and concrete material science. The electrochemical behavior of the embedded steel is discussed in correlation with microstructural characterization of the bulk cementitious matrix (the full scale of this experiment, including more details on electrochemical performance and the properties of the steel/cement paste interface are reported in (Koleva D.A. 2010a)

2.1 Experimental materials and methods

2.1.1 Materials

Reinforced concrete cylinders ($d = 700$ mm, $h = 200$ mm) were cast according EN 196-1, using water to cement ratio 0.6 (effective 0.48), cement to sand to gravel ratio 1:2:4.

The steel reinforcement (construction steel FeB500 HKN, $d=12$ mm, $h=200$ mm; composition according NEN6008 (in wt.%): C < 0.12 wt.%, Si max 0.6, P max 0.05, S max 0.05, N max 0.012) was cast as received. Both ends of the steel bars were isolated (to avoid crevice corrosion) and the bar was positioned in the middle of the concrete specimens. Embedded in

the concrete cover was a Mixed Metal Oxide (MMO) titanium mesh, serving as a counter electrode; SCE electrode was used as a reference electrode. The experimental set-up and specimen's geometry are as previously used and reported in (Koleva D.A., et al. 2007a). Two main groups of specimens are discussed: 1) mixtures, using OPC CEM I 42.5N; and 2) mixtures, using BFS cement CEM III/B 42.5N. Group 1) is denoted OPC, group 2) is denoted BFS. Table 1 summarizes the chemical composition of BFS and OPC cements, used in this study (supplier of the cements is ENCI, NL). All groups were cured for 28 days in fog room (20°C and 98% humidity) and then placed in lab conditions: lab air, 22°C and 1/3rd of height immersed in water (control groups) or 5% NaCl (corroding groups), 18 replicates per group and condition were monitored.

Chemical composition, wt.%		
Oxide	OPC	BFS
	CEM I 42.5	CEM III/B 42.5N
CaO	63.90	48.20
SiO ₂	21.00	30.10
Al ₂ O ₃	5.03	10.10
SO ₃	3.00	2.50
Fe ₂ O ₃	2.83	1.00
MgO	2.00	6.80
Na ₂ O	0.24	0.30
K ₂ O	0.65	0.30
TiO ₂	0.30	-
P ₂ O ₅	0.16	-
Mn ₂ O ₃	0.06	-

Table 1. Chemical composition of OPC and BFS (ENCI, NL)

2.1.2 Methods

Conventional monitoring: in terms of assessing corrosion initiation, a generally accepted method is half-cell potential mapping, hereby performed for the reinforced concrete cylinders according ASTM C876 and NACE RP0290-2000 respectively. Chemical analysis was performed for the cement paste adjacent to the steel surface in each technical condition according ASTM C1218 and ASTM C1152 for total chloride concentration in wt.% per dry cement weight (using Volhard titration method). The Electrochemical methods involved were electrochemical impedance spectroscopy (EIS) and potentiodynamic polarization (PDP). The measurements were performed at open circuit potential (OCP) for all cells. PDP was performed in the range of -0.15 V to +0.75 V vs OCP at scan rate 0.5 mV/s. The EIS measurements were carried out in the frequency range of 50 KHz to 10 mHz by superimposing an AC voltage of 10 mV. The used equipment was a High performance Autolab PGSTAT302N, combined with FRA2 module, using GPES and FRA interface. Scanning electron microscopy, using ESEM Philips XL30, combined with energy dispersive X-ray analysis (EDX) has been employed for visualization and microstructural investigations directly on the steel surface and on cross sections of the steel/cement paste interface. Section images of the specimens were obtained in backscattered electron (BSE) mode, operating at an accelerating voltage of 20 to 25 kV for imaging and EDX analysis. Image analysis was performed using OPTIMAS software package. Further, the combination of ESEM images and quantitative image

analysis allows deriving structural information of pore space, such as the porosity and critical pore size of the bulk cementitious matrix. On the basis of mathematical morphology transformations, pore size distribution can be obtained by using a sequence of similarly shaped structuring elements of increasing size (Serra J. 1982). The results from image analysis are an average of 35 locations per sample of 20 × 20 mm for the bulk matrix in each specimen. The physical size of the reference region of each image is 226 μm in length and 154 μm in width, with resolution of 0.317 μm/pixel, corresponding to a magnification of 500x; the sample preparation and imaging procedures are as reported in (Serra J. 1982, Ye G. 2003, Hu J. et al. 2003, Koleva D. A., et al. 2010b, Koleva D. A., et al. 2007b).

2.2. Results and discussion

2.2.1 Potential mapping

Figure 1 presents the evolution of Open Circuit Potentials (OCP) for the corroding cells from groups OPC and BFS with time of conditioning (the OCP values for the identical in preparation and geometry, but immersed in water, control groups OPC and BFS were always more noble than -250 mV SCE).

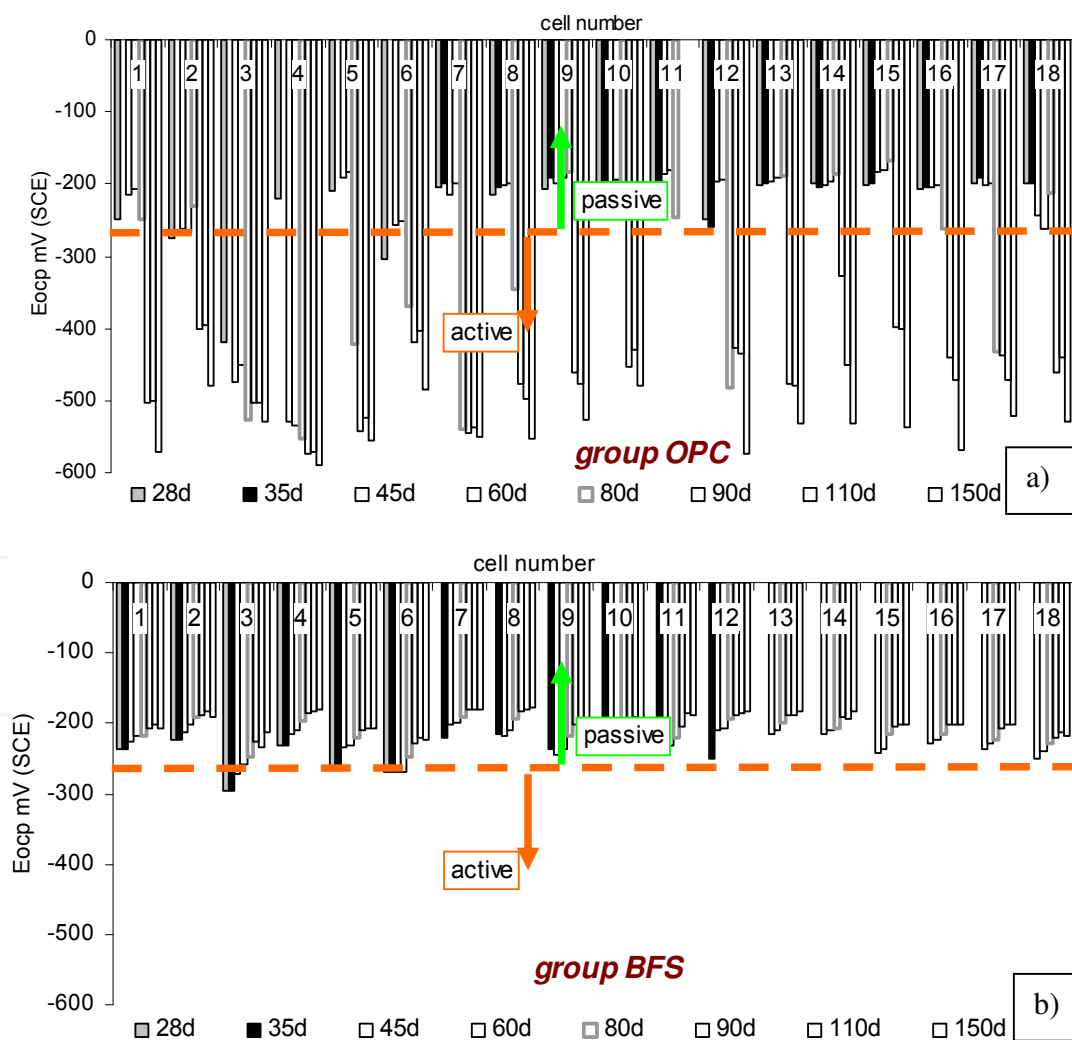


Fig. 1. Evolution OCP values for the corroding OPC and BFS specimens with time

Relevant to steel in reinforced concrete (and according ASTM C876) the evolution of OCP values gives information for the time to corrosion initiation, following the criteria: $E_{ocp} > -270$ (SCE) mV is interpreted as minimum probability for steel corrosion i.e. passive state, whereas $E_{ocp} < -270$ mV(SCE) means high probability for corrosion or active corrosion state. The OCP values in Fig. 1, refer to the stages from 28 to 150 days after immersion in 5% NaCl. As seen from the plots at the latest stage of 150 days, all OPC cells exhibit active corrosion behavior with OCP values between -500 to -600 mV (Fig.1a). In contrast, the “corroding” cells from BFS group (Fig. 1b) exhibit OCP values above the threshold for active corrosion i.e. all cells show no evidence of active corrosion (i.e. $E_{ocp} > -270$ mV SCE) for the hereby presented duration of test of 28 - 150 days.

2.2.2 Potentio-dynamic polarization (PDP)

Figure 3 depicts an overlay of PDP curves for all investigated cases (control and corroding OPC and BFS specimens) for 28 days (first recorded time interval) and 150 days (latest recorded time interval). As seen from the plots, at 28 days similar corrosion potentials (E_{corr}), anodic currents and corrosion current densities (I_{corr}) respectively are recorded for all cases, with a more active behaviour for the corroding OPC and BFS cells and the control BFS cells. At the stage of 150 days corrosion was observed only for the corroding OPC specimens, while all other groups behave similarly to the 28 days stage: the most significant anodic control in the region immediately after E_{corr} is observed for the control specimens OPC, followed by the control and corroding specimens BFS, whereas the corroding specimens OPC present significantly higher corrosion and anodic current densities and cathodically shifted corrosion potential i.e. at the stage of 150 days corrosion is still not initiated in the BFS corroding group. Corrosion current density values (I_{corr} , $\mu\text{A}\cdot\text{cm}^{-2}$) for the control and corroding OPC and BFS groups were calculated after IR drop correction and using Tafel and Butler-Volmer equation fit of the Autolab interface. The I_{corr} values for the control groups (OPC and BFS) and for the corroding BFS group are very low (lower than $0.1 \mu\text{A}\cdot\text{cm}^{-2}$), whereas active behaviour and corrosion current density of approximately $0.4 \mu\text{A}\cdot\text{cm}^{-2}$ (and increasing) is relevant for the OPC corroding group.

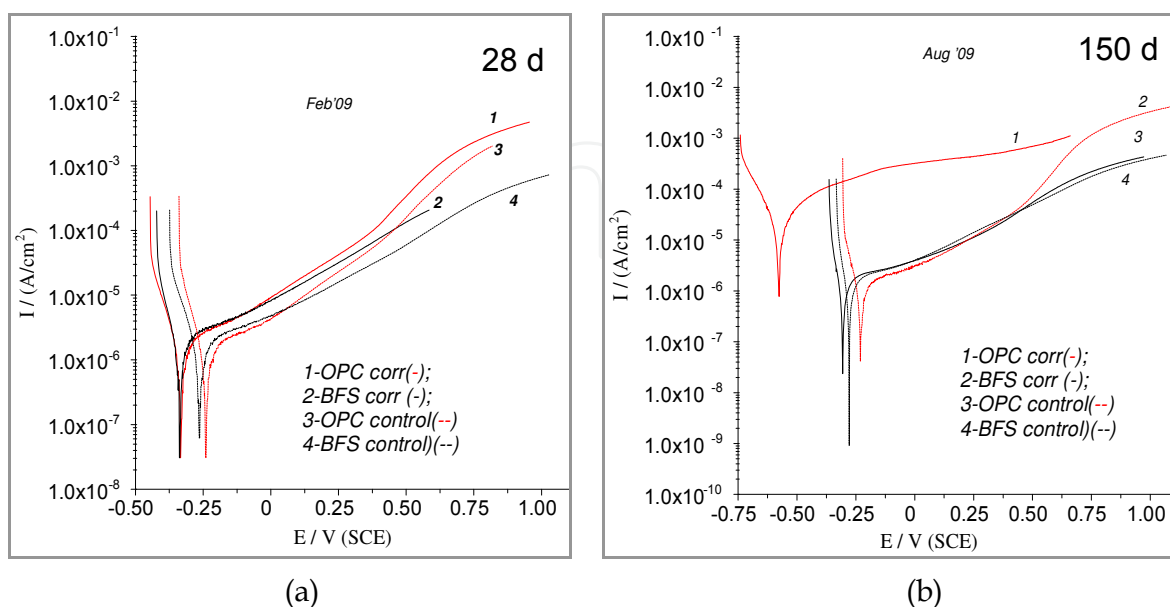


Fig. 2. PDP curves for OPC and BFS control and corroding groups at 28 (a) and 150 (b) days

2.2.3 Electrochemical impedance spectroscopy (EIS)

EIS is a useful technique for obtaining knowledge of the steel/concrete system as it provides information for both the steel surface (electrochemical parameters) and the concrete bulk matrix (concrete bulk and pore network resistance) (Sagüés A. A., et al. 1995, Feliú V., et al. 2004). Figure 3 depicts the equivalent electrical circuit, used for interpretation and data fitting of the experimental EIS response (the circuit is as previously used and reported in (Koleva D.A., et al. 2007a, Koleva D. A., et al. 2009).

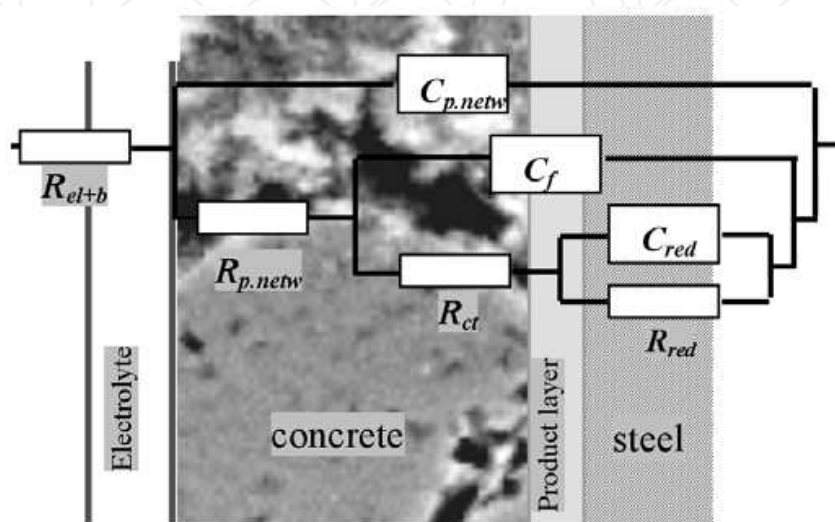
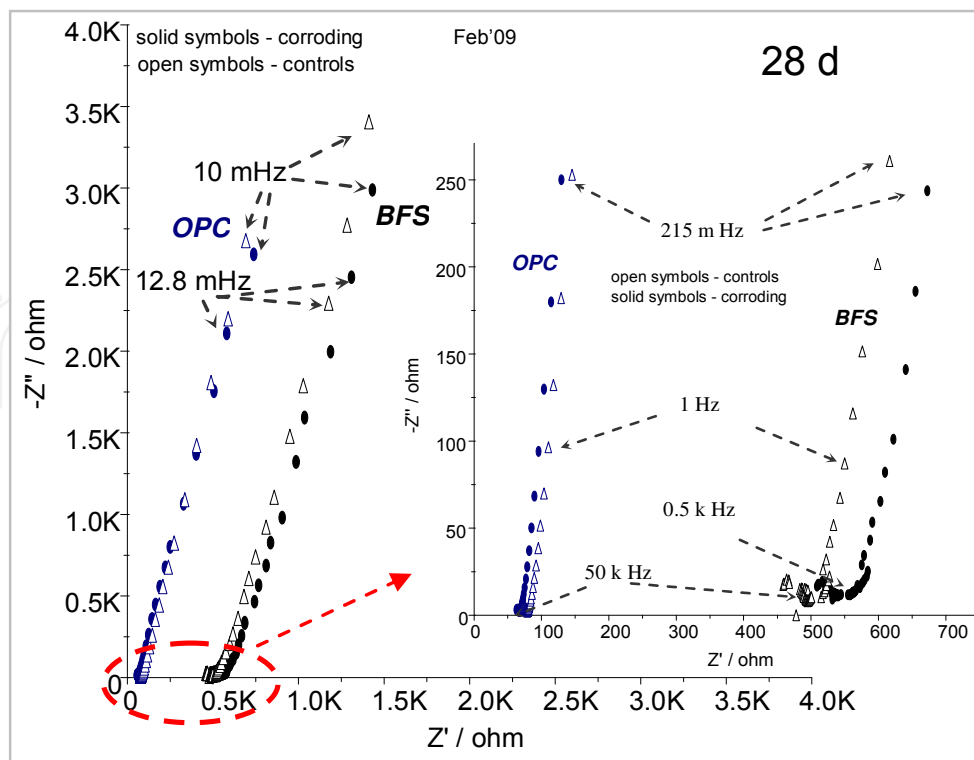


Fig. 3. Equivalent electrical circuit for fitting the experimental EIS response

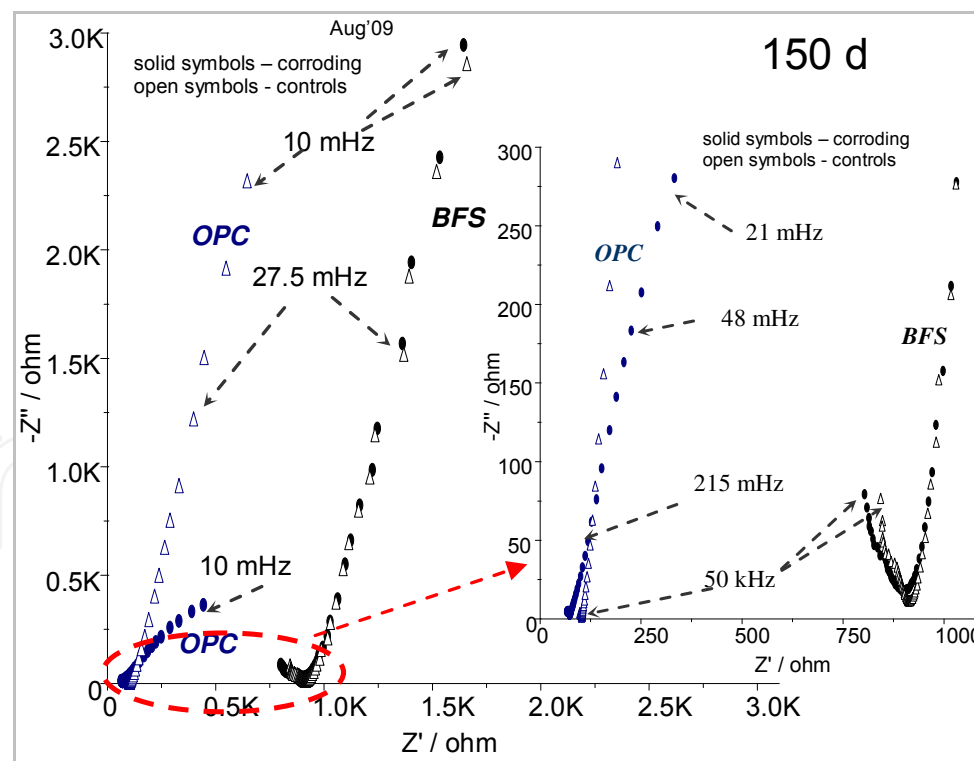
The elements of the equivalent circuit present the following physical meaning: R_{el+b} is the concrete resistance including the contribution of electrolyte resistance, the latter being negligible compared to the concrete resistance. The first time constant ($R_{p.netw}, C_{p.netw}$) is attributed to the properties of the concrete matrix in terms of pore network; the second time constant (R_{ct}, C_f) deals with the electrochemical reaction on the steel surface; the third time constant (R_{red}, C_{red}) is attributed to redox processes, taking place in the product layers on the steel surface. An overlay of the experimental EIS response in Nyquist format for all groups is presented in Fig. 4 relevant to the time intervals of 28 (Fig. 4a) and 150 days respectively (Fig. 4b). Summarised data for the best fit parameters are presented in Table 2.

The high frequency response corresponds to the concrete bulk resistance, including the contribution of electrolyte resistance. The obtained ($R_{b+p.netw}$) values (Table 2) correspond to the overall concrete resistance. For deriving polarization resistance (R_p) from EIS measurements in reinforced concrete (R_{ct} and R_{red} respectively), the medium-low and low frequency limits of the impedance spectra are generally considered, as reported in (Montemor M. F., et al. 2002, Feliú V., et al. 1998, Wenger F., et al. 1990, Fedrizzi L., et al. 2005), previously discussed and reported for reinforced mortar and concrete in (Koleva D.A., et al. 2007a, Koleva D. A., et al. 2009) and used in the present study as well.

At the stage of 28 days similar EIS response in terms of electrochemical behavior was recorded for all cells, evidenced by the close to capacitive behavior at low frequencies (indicating situation of passivity). The result is in line with the PDP curves (Fig. 2a) for this time interval. The response for all OPC and BFS specimens (for all stages) differs in the high frequency domain, denoted to the bulk properties of the cement-based matrix in BFS, compared to OPC. The former matrix is generally reported to be denser compared to the



(a)



(b)

Fig. 4. EIS response at 28 days (a) for corroding OPC and BFS (solid symbols) and for control OPC and BFS (open symbols); EIS response at 150 days (b) for corroding OPC and BFS (solid symbols) and for control OPC and BFS (open symbols)

latter one (Bouikni A. et al. 2009, Giorv O. E., et al. 1979, Manmohan D., et al. 1981, Kumar A.D.M. 1986, Hooton R.D., 1986), which gives the difference in bulk matrix resistance, Table 2 (about 300 kOhm.cm² for the BFS groups, compared to approximately 50 kOhm.cm² for the OPC groups at stage 28 days). Figure 4b presents the latest stage of the experiment, 150 days, reflecting still passive state for the corroding BFS group and enhanced corrosion activity for the OPC corroding group only (reduced magnitude of |Z| and phase angle drop to below 40°). Table 2 summarizes all best-fit parameters (for 28 and 150 days). The bulk matrix resistance ($R_{b+p.netw}$) for all specimens (corroding and control groups) increases with time as a result of cement hydration (NaCl slightly influencing the electrical resistivity values), the major difference being denoted to the type of cement i.e. OPC cells (corroding and control) presenting bulk matrix resistance in the range of 55 – 86 kOhm.cm², while for BFS cells, this range is 460 - 470 kOhm.cm² at 150 days.

Time interval	R_{el+b} kOhm.cm ²	$R_{p.netw.}$ kOhm.cm ²	$C_{p.netw.}$ μF/cm ²	$R_{ct.}$ kOhm.cm ²	C_f μF/cm ²	$R_{red.}$ kOhm.cm ²	C_{red} μF/cm ²	$R_{b+p.netw.}$ kOhm.cm ²
OPC corroding								
28 d	34.98	17.75	2.31	76.90	32.56	817.30	26.92	52.74
150 d	38.65	16.51	1.36	14.59	76.92	48.67	229.49	55.16
OPC control								
28 d	39.42	10.58	1.16	81.92	35.26	869.20	27.56	50.00
150 d	53.25	33.69	2.19	87.36	26.79	1237.40	25.00	86.95
BFS corroding								
28 d	275.03	26.99	3.88E-02	78.39	29.49	984.36	34.62	302.01
150 d	409.70	57.95	1.94E-03	59.28	21.15	1184.82	29.49	467.65
BFS control								
28 d	238.39	22.39	1.94E-03	55.38	22.95	889.78	31.41	260.79
150 d	423.12	51.34	1.94E-03	84.24	26.15	1224.60	27.31	474.46

Table 2. Best-fit parameters, derived on basis of experimental EIS results, using simulation and fitting procedures and the equivalent circuit: $R_{el+b}(C_{p.netw}(R_{p.netw}(C_f(R_{ct}(C_{red}R_{red}))))$ (relative error for each best-fitted parameter 0.2 to 3.0%)

The charge transfer resistance (R_{ct}) decreases for the OPC corroding cells only (attributed to enhanced corrosion activity in this group), whereas no active behaviour is observed for the BFS corroding group, the latter behaving as a control group (the best-fit parameters in Table 2 are an average of 18 replicates per group). Considering the investigated system, the proposed equivalent circuit (Fig. 3) and the derived best-fit parameters (Table 2) the following can be summarized: the first time constant ($R_{p.netw}C_{p.netw}$) is related to the pore network of the bulk matrix since the capacitance values are low (range 0.002 to 2.4 μF.cm²), hence can not be denoted to electrical double layer on the steel surface or to redox-reactions (Feliú V., et al. 2004, Dhoubi L., et al. 2002). The second time constant ($R_{ct}C_f$) is related to the charge transfer resistance and double layer capacitance at the steel surface, since the capacitance is more or less stable with time for the control groups and increases for the corroding groups, which is consistent with the drop in charge transfer resistance for the latter groups. The third time constant ($R_{red}C_{red}$) is relevant to the transformations and contribution of the product layers on the steel surface; capacitance vales for the corroding group OPC being significantly higher than the control groups, attributed to the spreading of corrosion damage on a larger steel surface area with time of conditioning.

The data derived from potential mapping, PDP and EIS tests of OPC and BFS corroding and control specimens denote for active corrosion state in the OPC corroding group only. In contrast, the BFS corroding group behaves as a control one. According to electrochemical behavior, steel corrosion in this group is still not initiated at the stage of 150 days. Obviously, the altered microstructural properties of BFS containing specimens play a significant role in corrosion delay. In order to verify this statement and elucidate the reasons for the observed electrochemical behavior, a bulk matrix investigation is required, which will be discussed in the following sections.

2.2.4 Bulk matrix properties

The previously discussed electrochemical behaviour is supported by wet chemical analysis for chloride concentration in the cement paste, adjacent to the steel surface. The analysis was performed in a way as schematically shown in Fig. 5 (bottom, middle and top of the cylinders). The result is approximately 5 times higher chloride concentration (in wt.% per dry cement weight) in the OPC corroding cells, compared to the BFS corroding cells. Two considerations are hereby relevant: on one hand, the matrix permeability of the BFS cells is most likely significantly lower; secondly, although low, the chloride concentration in the BFS cells is at the threshold for corrosion initiation (accepted to be between 0.2 and 2 wt%, (Pettersson K. 1994, Page C. L. 2002, Vassie P.R.W. 1984, Glass G.K., et al. 1997)), yet corrosion in the BFS cells was not observed. Apparently, not only chemical composition, but also the microstructural properties of the matrix play a distinctive role for the corrosion initiation (or lack thereof) and electrochemical behaviour of the embedded steel. The delay in corrosion initiation in the BFS specimens (as evidenced by potential mapping, PDP and EIS response) is attributed to a modified cement-based matrix. As a result, at 150 days of conditioning, chlorides are not yet present at the steel/cement paste interface and corrosion in the BFS specimens is still not initiated within the hereby investigated period.

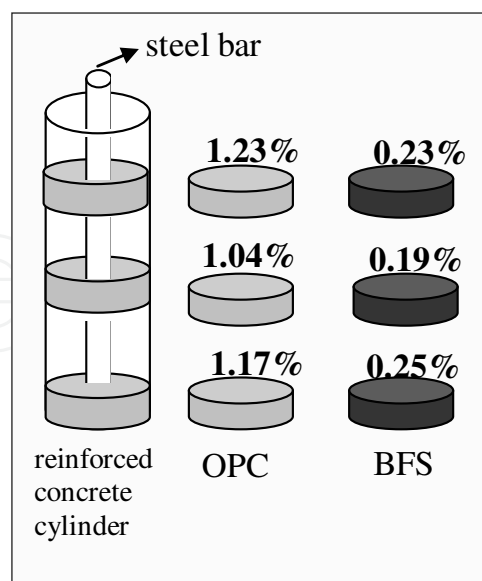
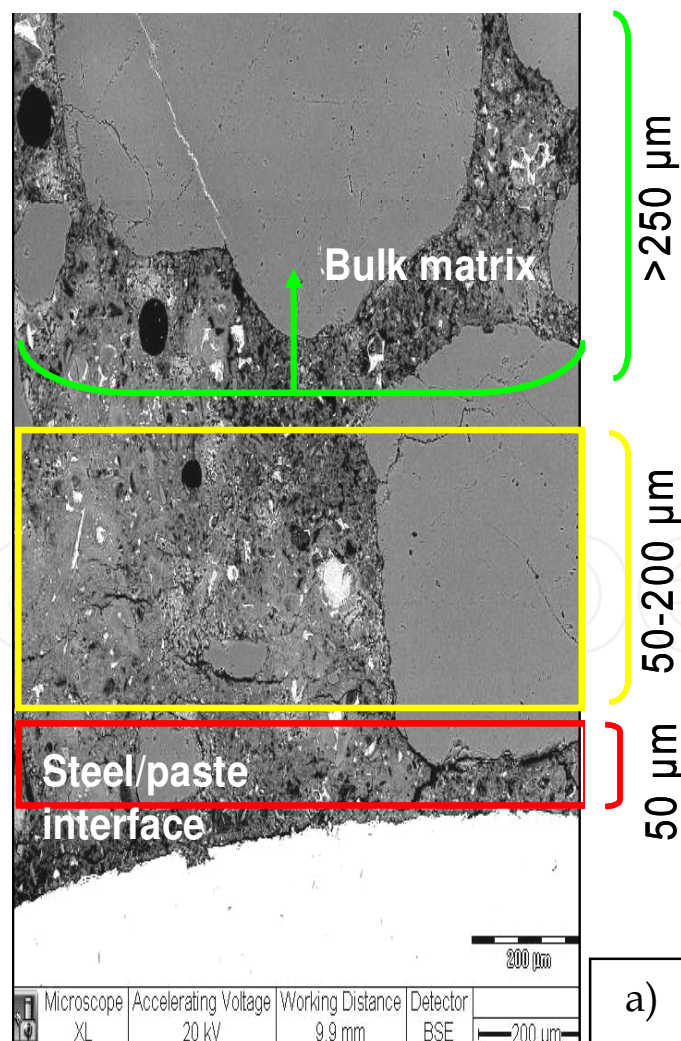


Fig. 5. Schematic presentation of the reinforced concrete cylinders and the location of the samples, taken from each investigated case for chloride wet chemical analysis and chloride concentration in wt.% per dry cement weight (for each specimen type, the samples are taken from identical locations of the cylinders)

With respect to microstructure of the bulk matrix, there are three main mechanisms/processes, influencing the microstructural properties: cement hydration with aging, the influence of NaCl, which accelerates cement hydration and causes initial densification of the bulk porosity (Suryavanshi A.K., et al. 1995, Díaz B., et al. 2006), and third - the corrosion process itself (volume expansion of corrosion products induces micro-cracking). Since reinforced concrete is a highly heterogeneous material and considering the variety and complexity of external influences in this study, it is inappropriate to claim absolute values for each parameter. Hence, the analysis would be better considered as comparative investigation between the different concrete mixtures and regimes of conditioning, based on the fact that all investigations were performed in exactly the same manner for each specimen.

2.2.5 Bulk matrix microstructure: fundamental aspects

The electrolytic path in reinforced cementitious systems is dependent on the kinetics of ion transport mechanisms. These mechanisms, in addition to the cement hydration and the morphological alterations, are affected by the pore size distribution and the pore connectivity of the bulk concrete material. The original BSE image (or a selected area, similar to the presented in Fig. 6a micrographs, provided the analysis should exclude the aggregate



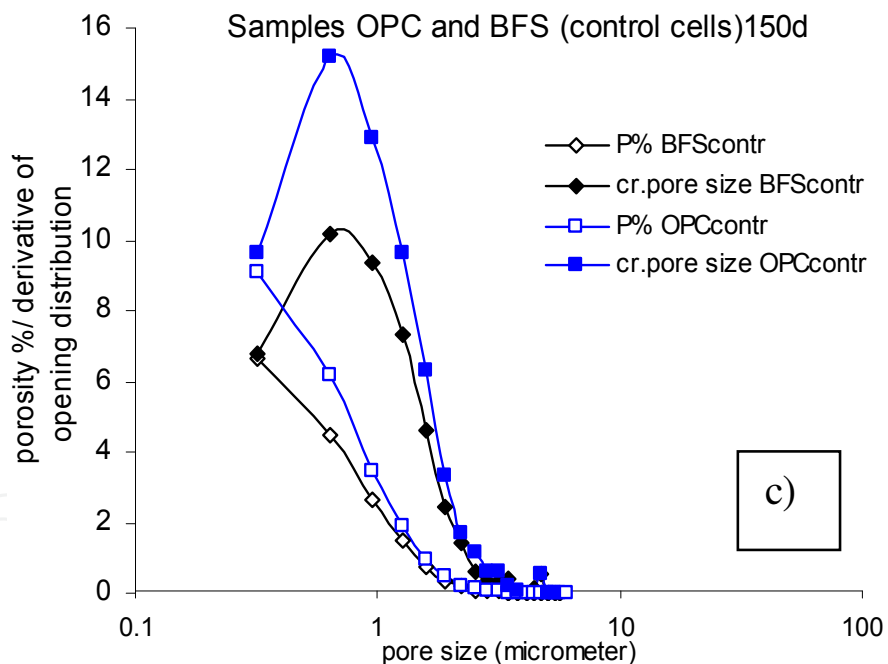
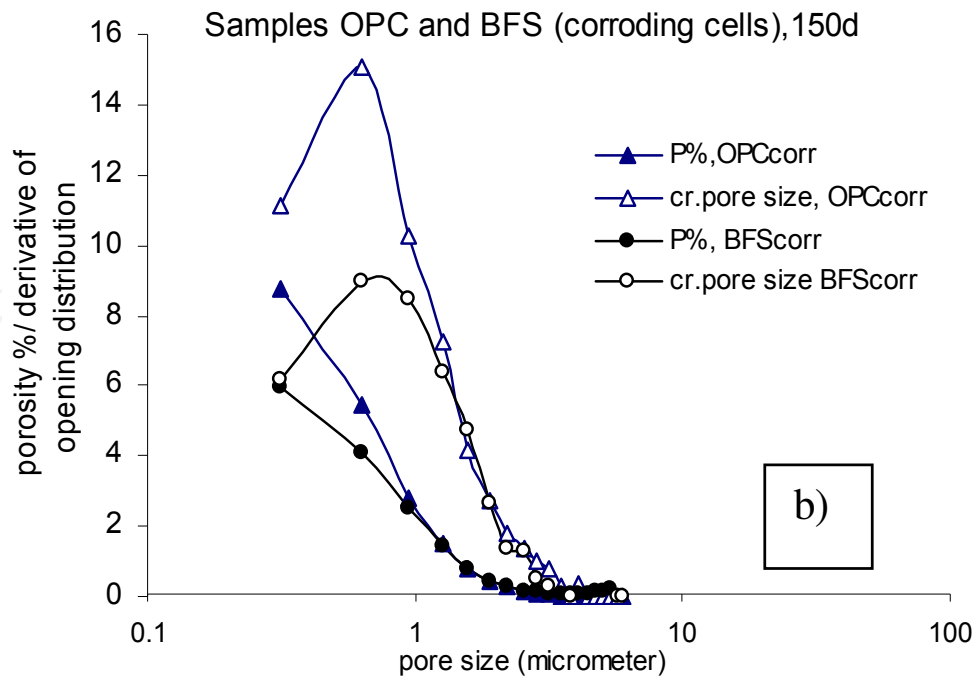


Fig. 6. SEM micrographs (mounted images) of the steel/cement paste interface and into the bulk matrix (a); porosity/pore size distribution for corroding groups OPC and BFS (b) and control groups OPC and BFS (c)

particles in the image, if any) is segmented by applying a gray-level threshold to create a binary image, reflecting the pore phase (Ye G. 2003). The binary image is then subjected to quantitative image analysis for derivation of structural parameters (pore size distribution, critical pore size, pore connectivity etc.). The “opening distribution” technique was used, whereby the binary image is opened by a series of squares of increasing size (Hu J. et al.

2003). The cumulative pore size distribution curve is obtained by plotting the pore area fraction after an opening operation versus linear dimension of the structuring element (as presented in Fig. 6b)c)). This gives a type of "size" classification in the case of an interconnected structure, like pore space in concrete. The critical pore size l_c can be conceived as the diameter of the pore that completes the first interconnected pore pathway in a network, developed by a procedure of sequentially adding pores of diminishing size to this network. The critical pore size l_c is a unique transport length scale of major significance for permeability properties and can be associated with the inflection point of the cumulative pore size distribution curve (Fig. 6b)c)).

In this research, relevant to morphological aspects of the pore structure and ion transport, the pore interconnectivity (defined as the fraction of connected pores out of the total pore area) is used in terms of pore distribution density (PDD), as PDD contains information on both pore size and connectivity of pore space and gives the permeability of the matrix. For more details on the fundamental aspects and image analysis of cement-based materials, including mortar, plain concrete and reinforced concrete, please see (Serra J. 1982, Ye G. 2003, Hu J. et al. 2003, Koleva D. A. 2007c).

2.2.6 Correlation of pore structure characteristics and EIS parameters

A set of SEM images on polished sections were made and were further subject to image analysis. The hereby discussed porosity and pore size distribution refer to the bulk matrix only. The structural parameters were averaged from at least 35 locations in the bulk matrix (sample of 2x2 cm). The final data were considered after performing a statistical evaluation in terms of frequency of occurrence (% distribution) vs class (porosity in %) for the samples in each regime. The calculated pore size distribution and critical pore size are presented in Fig.6b)c) for the bulk matrix (> 250 μm away from the steel surface) for specimens groups OPC and BFS corroding (b) and OPC and BFS control (c). The highest bulk porosity was recorded for the control specimens OPC (9.06 %), followed by the corroding OPC specimens (8.78%). The lowest porosity was observed for the corroding specimens BFS (5.92%), the control BFS specimens exhibiting slightly higher porosity of 6.62%. The critical pore size for all investigated groups is similar (approximately 0.634 μm). The porosity difference between OPC and BFS corroding (and control) specimens (of 2-3%) could not be responsible for the significantly lower chloride concentration in the corroding BFS, compared to corroding OPC groups (Fig. 5). Apparently porosity alone is not the factor determining the significantly different electrochemical behavior (Figs. 1, 2 and 4), delayed chloride ingress and corrosion initiation respectively in the BFS corroding cells. What has to be considered is the pore interconnectivity in the cement-based matrix and thus the matrix permeability. Figure 7a) presents the derived from image analysis (for hydration stage 150 days) porosity and matrix permeability.

As seen from the plot, the almost equal porosity in specimens OPC control and OPC corroding (higher than both BFS groups) does not result in similar pore interconnectivity and permeability respectively. The specimens OPC corroding are characterized with lower permeability (8.02×10^{-10} m/s), compared to specimens OPC control (1.29×10^{-9} m/s). The result for the former case is denoted to the influence of NaCl, which initially accelerates cement hydration and leads to a larger portion of isolated and/or disconnected conductive paths (Koleva D. A., et al. 2007b, Suryavanshi A.K., et al. 1995, Díaz B., et al. 2006, Koleva D. A., et al. 2008b, Koleva D. A., et al. 2008c). At this stage steel corrosion is at a low to moderate stage (as evidenced by the derived corrosion current densities for the group OPC

corroding), hence a significant contribution of micro-cracking due to volume expansion of corrosion products at the steel/cement paste interface is not observed. Therefore, the permeability of the corroding specimens OPC ends up still lower than the control specimens OPC. Figure 7a) depicts the slightly lower porosity values for both control and corroding groups BFS, but significantly lower (than the OPC groups) permeability values ($\sim 4 \times 10^{-10}$ m/s).

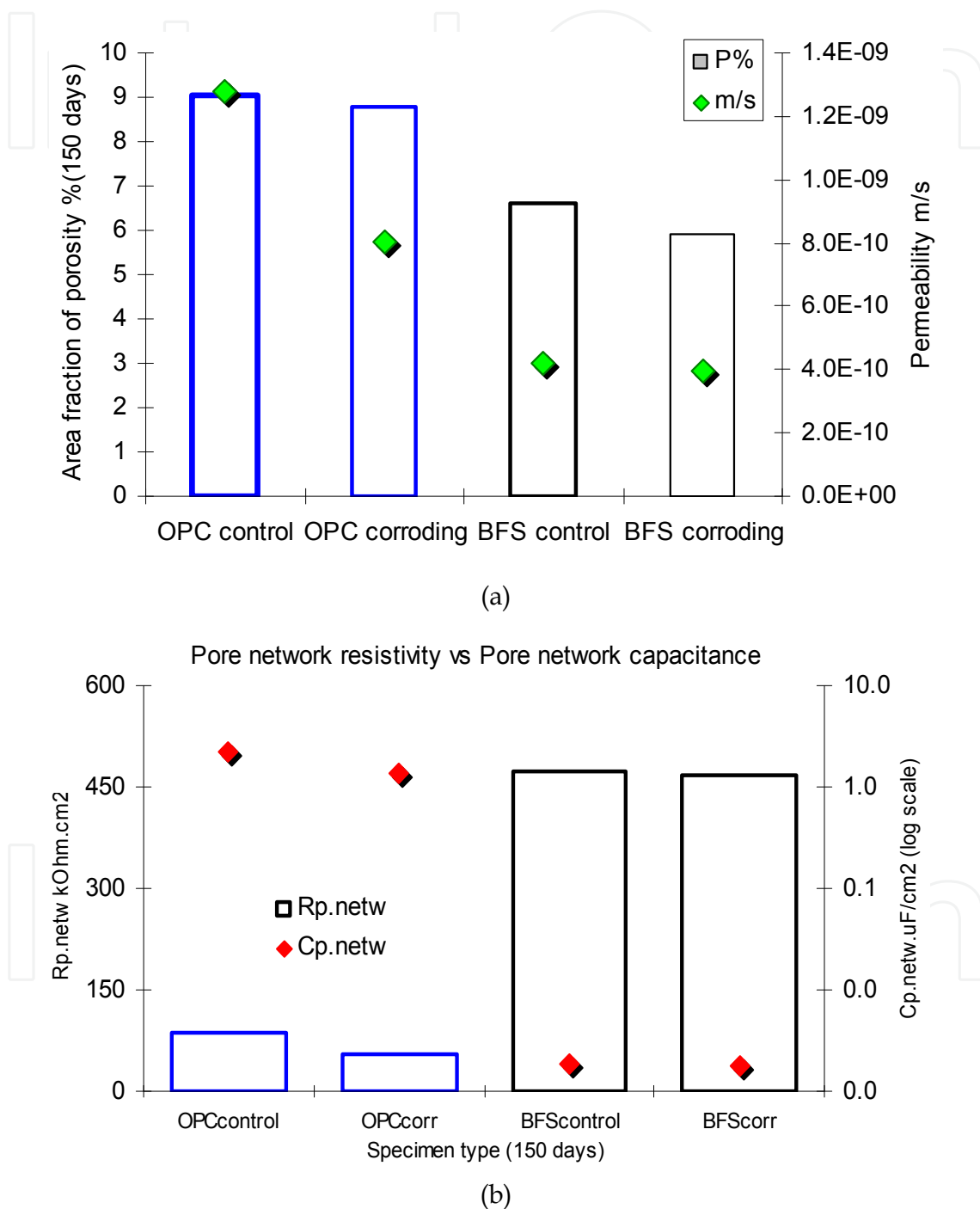


Fig. 7. (a) correlation of porosity (%) and permeability (m/s), derived from image analysis for all investigated groups at the stage of 150 days; (b) Pore network resistivity versus pore network capacitance (as derived by EIS) for all studied groups, stage 150 days

Further, a correlation can be made between pore network parameters (Fig. 7a) and electrochemical (EIS) parameters, mainly pore network capacitance ($C_{p.netw}$) and pore network resistance, $R_{p.netw}$ (Fig. 7b). The higher porosity (P%) and permeability (m/s) in OPC control and corroding cells (Fig. 7a) corresponds to the highest $C_{p.netw}$ and lowest $R_{p.netw}$ (Fig. 7b), the values being lower for OPC corroding cells, compared to OPC control cells (Fig. 7b). The lowest $C_{p.netw}$ ($1.94 \times 10^{-3} \mu\text{F.cm}^{-2}$, Fig. 7b) corresponds to the lowest permeability values, derived for specimens BFS (both corroding and control groups, Fig. 7a). The result is very well in line with the derived global bulk electrical resistivity of the matrix in BFS as well (Table 2). Consequently, the BFS matrix in the corroding specimens would be characterized with a larger pore surface area but also increased portion of disconnected and isolated conductive pore pathways (increased pore network resistance). The capacitance values for BFS corroding cells are significantly lower than those for the OPC corroding cells, therefore a comparison of pore network permeability and interconnectivity between OPC and BFS specimens can be reliably derived on the basis of pore network capacitance and resistance. Consequently (and moreover, after verification with microstructural analysis), it can be stated that EIS is a powerful, non-destructive technique for evaluation of pore network parameters. Combined with the electrochemical parameters, derived for the embedded steel, EIS allows a thorough evaluation of a reinforced concrete system.

Summarizing, this paragraph discussed the corrosion behaviour of reinforcing steel in OPC and BFS concrete, subjected to chloride-induced corrosion (5% NaCl), in comparison with control cases for both concrete types. Additionally, the electrochemical parameters for the embedded steel were correlated with the microstructural parameters and properties of the bulk concrete matrix. After 150 days of conditioning, corrosion was not initiated in the BFS reinforced concrete, whereas active behavior was observed (starting at 40 - 45 days) for the steel in OPC concrete. The higher corrosion resistance in BFS reinforced concrete is denoted to decreased pore-network interconnectivity, evident from the significantly lower pore network capacitance and higher pore network resistance, as derived from EIS and verified on the basis of microstructural analysis. In that sense EIS appears to be a valuable tool for non-destructive and thorough evaluation of not only the electrochemical behavior of reinforcing steel, but also for detailed investigation of the bulk cement based matrix.

3. OPC reinforced mortar, using red mud as partial cement replacement

Corrosion in reinforced concrete is a major and costly concern, arising from the higher complexity of involved phenomena on different levels of material science (electrochemistry, concrete materials, etc.) and material properties (macro/micro/ nano). As previously introduced, for a thorough evaluation of a reinforced cement-based system (as reinforced concrete) an integrated approach of electrochemistry and concrete material science is necessary in order to thoroughly evaluate corrosion-related phenomena. Moreover, when a modified cement-based material is to claim superior performance, the synergy of various fundamental aspects and experimental tests is a must.

This paragraph deals with a brief introduction of a sustainable solution for corrosion control in reinforced concrete, by using a waste from the aluminium production (i.e. Red Mud), as partial replacement of the cement fraction in the reinforced concrete system (for the elaborated and complete work on red mud-containing mortar and concrete, please see (Koleva D.A. 2011)). The waste "red mud" (RM) is generated during aluminium production

from bauxite. The annual production of 1 tone of metallic aluminium generates about 2 tones of red mud (Ayres R.U, et al. 2001). The disposal of this alkaline waste is expensive (up to 1–2% of the alumina price); the enormous quantity of red mud generated every year (about 66 million tones) poses very serious and alarming environmental problems (Mymrin V., et al. 2003). Consequently, research on ways of making use of this residue is of significant importance.

Red mud is reported to increase steel passivity in alkaline solutions (pre-treatment procedure) (Collazo A., et al. 2007, Díaz B., et al. 2004); “red mud” additions to cement-based materials are reported to result in mixtures, shielding X-ray radiation or heavy metal (and other toxic substances) binding effects (Amritphale S.S, et al. 2007, Cengelolu Y, et al. 2007, Yong Liu, et al. 2007), while maintaining sufficient mechanical properties (Tsakiridis P.E., et al. 2004).

To this end, the objective of an ongoing research project is to investigate the application of “red mud” as an additive for reinforced concrete, aiming to achieve corrosion protection on one hand, to eventually improve the concrete bulk microstructure on the other and thus to finally contribute to cement cost reduction and waste utilization in an ecologically friendly manner. This paragraph reports on the electrochemical behaviour of steel in red mud-modified mortar and the microstructural characteristics of the bulk matrix. Further, an illustration for the recorded superior steel corrosion performance in the presence of wastes is provided by means of microscopical analysis and x-ray techniques (the recorded parameters for the full duration of the test of 310 days, including X-ray tests (XRD and XRF) and a detailed presentation of the electrochemical measurements is reported in (Koleva D.A. 2011)). The aim of this paragraph is to add clarification and give another example (in addition to paragraph 2) for the implementation of electrochemistry and concrete material science in evaluating a reinforced cement-based system, particularly in the presence of wastes.

3.1 Experimental materials and methods

Materials: Reinforced mortar cylinders ($d = 3.5$ cm; $h = 20$ cm) were cast from OPC CEM I 32.5, cement/sand ratio of 1:3 and water/cement ratio of 0.5. Four groups (5 replicates per group) were monitored: two control groups (non-corroding) with and without red mud, denoted as RMw and OPCw respectively, and two corroding groups, with and without red mud, denoted RMn and OPCn. All specimens were cured for 7 days in fog room (20 °C and 98% RH) and maintained in lab air further on. An external solution of 10 % NaCl was used as a chloride-induced accelerator for the corroding groups (the specimens were 1/3rd of height immersed in the solution; the control specimens were immersed in tap water). Red mud was added (after drying at 105°C and grinding to cement finesse) as a 20% cement replacement for the RMw and RMn specimens. The chemical and mineralogical composition of red mud depends on the processed bauxite, the aluminium production process itself and the geographical location (Li L.Y 1998). The red mud used in this study was supplied from Suriname (XRF analysis of the received supply gives major contributions of: Al₂O₃ 29.1 wt.%, Fe₂O₃ 24.9 wt.%, Na₂O 14.3 wt.%, SiO₂ 20.2 wt.%, CaO 3.5 wt.%). The steel re-bars (construction steel FeB500 HKN, $d=0.8$ cm, $h=10$ cm) were embedded “as received” i.e. there was no preliminary treatment of the bars before casting (casting procedures, cement composition (OPC CEM I) and steel properties are as previously described with relevance to paragraph 2). **Methods:** The electrochemical methods, microscopical investigation and

image analysis employed in this part of the study are as previously listed in paragraph 2, section 2.1.

3.2 Results and discussion

3.2.1. Electrochemical behaviour

Open circuit potential (OCP) mapping and steel response with external from 7 days (initial lab conditioning) until 136 days are presented as follows. Figure 8 depicts the potential/time history (data interpretation as previously discussed in paragraph 2 and according ASTM C876) for two of the 5 replicates per specimens' group.

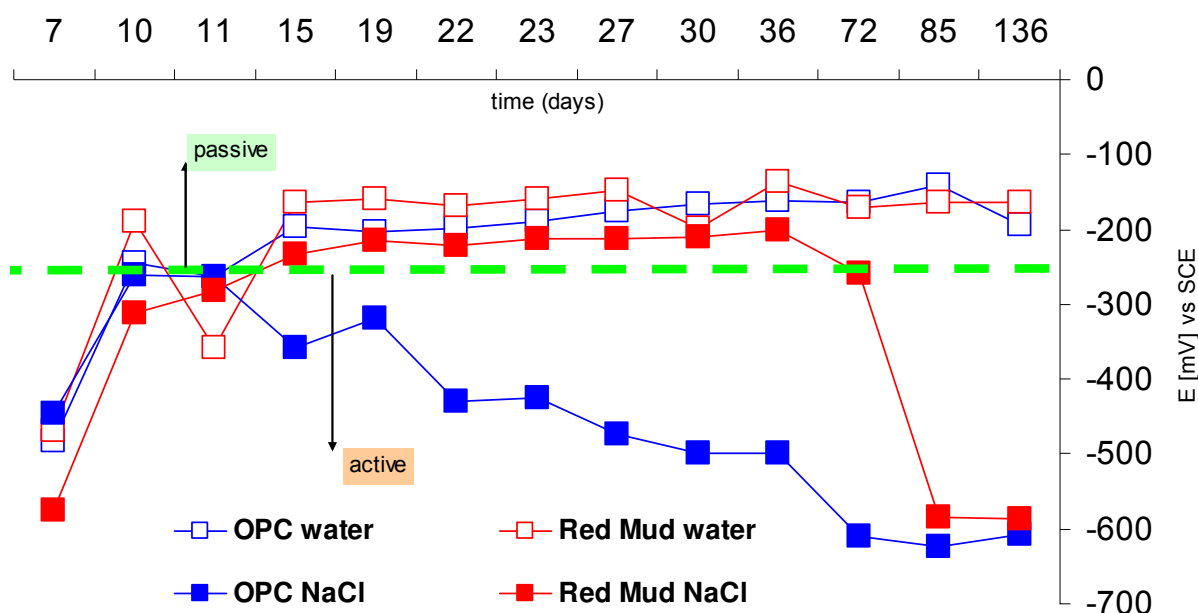


Fig. 8. OCP readings for corroding (OPC NaCl and RedMud NaCl) and control (OPC water and RedMud water) reinforced mortar from initial (7 days) until 136 days of treatment

As seen from the plot, an initially active behavior was observed for all cells (Fig. 8, 7 days stage), which actually corresponds to the end of the mortar “fog room” curing and the start of the lab conditioning (water for the control cells and 10% NaCl immersion for the corroding cells). Fundamentally this initial activity is due to the presence of galvanic micro-cells on the steel surface, formed as a result from steel heterogeneity (cathodic and anodic areas). Further, formation of the passive film takes place (starting 10-15 days) and as long as it remains intact, there will be no activity on the steel surface. In the event of chloride ions penetration through the mortar bulk matrix and arrival at the steel/cement paste interface (as in the case of specimens OPC NaCl, Fig. 8), corrosion will be initiated due to the disruption of the passive film in the presence of chlorides. What is interesting to note is the OCP evolution of the red mud containing corroding specimens (RM NaCl): in the period of 15 to 72 days of conditioning they behave as control (non corroding) cells, since their OCP values are more anodic than ~ -300 mV (SCE), whereas active corrosion was observed in the corroding OPC (OPC NaCl) specimens, which exhibit significantly lower (more cathodic) potentials. In other words, OCP evolution shows the significant corrosion delay in the presence of RM, which is further supported by the potentiodynamic polarization (PDP) tests (Fig. 9).

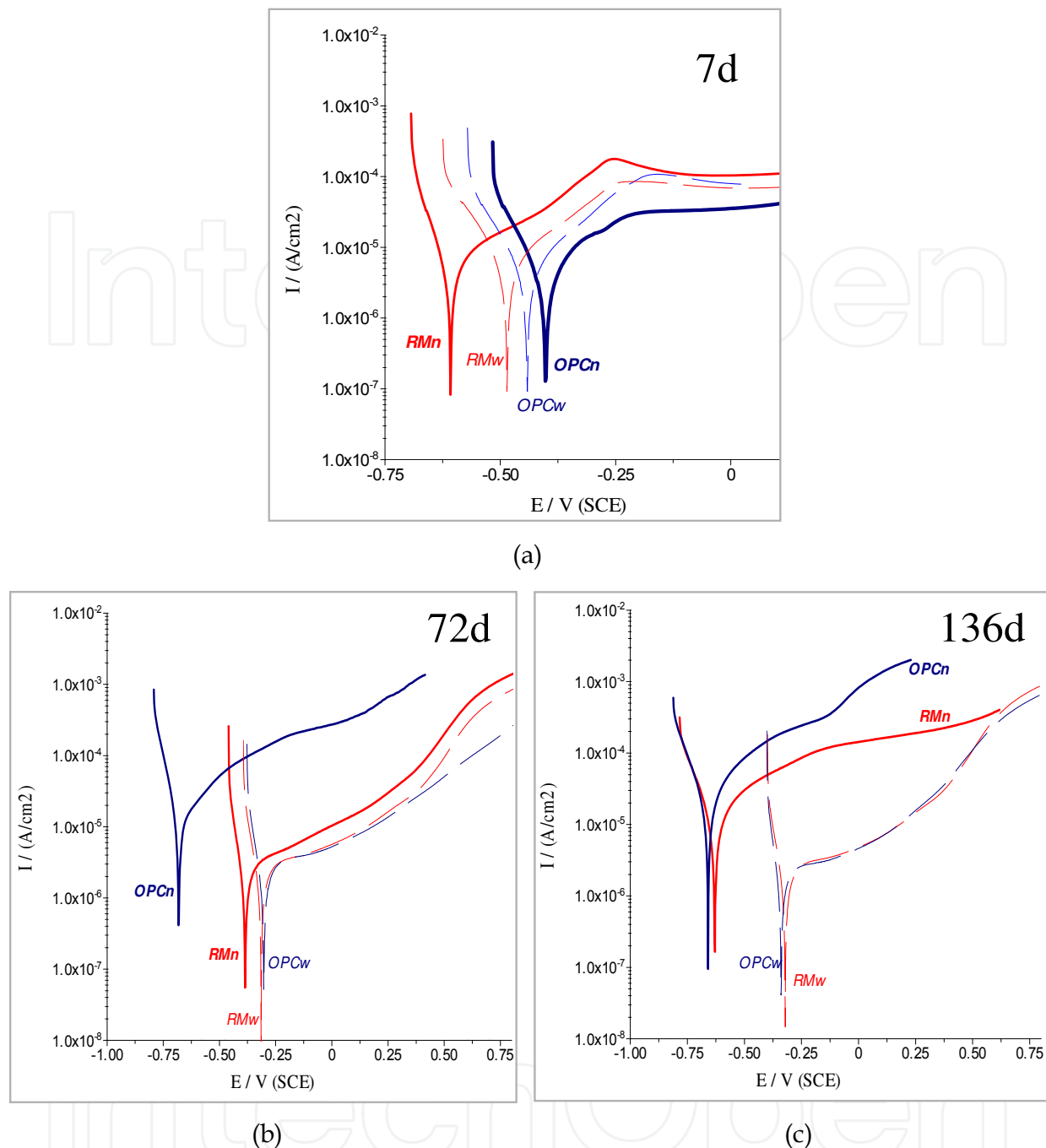
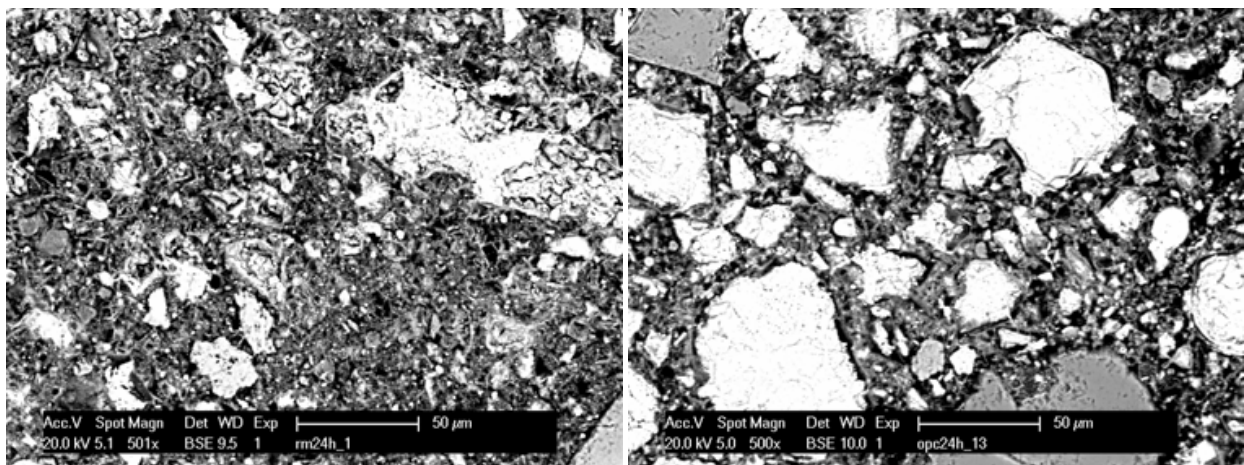


Fig. 9. PDP scans for all hereby investigated cells after 7 days (a), 72 days (b) and 136 days (c) of treatment

PDP was performed on intervals for all investigated specimens. Figure 9 depicts an overlay of PDP scans for all investigated groups at 7 days (a), 72 days (b) and 136 days (c). As seen from the plots, initially the RM containing groups present a slightly more active behaviour, corresponding to the initial alterations in the passive layer as previously discussed and recorded via OCP mapping (Fig. 8). Further and until 72 days (Fig. 9b) passive state was observed for the control OPCw and RMw cells, along with passive state for the corroding otherwise RMn(NaCl) specimens. The behaviour of the former two groups is as expected; for the latter group, although a transition from passive to active behaviour would be

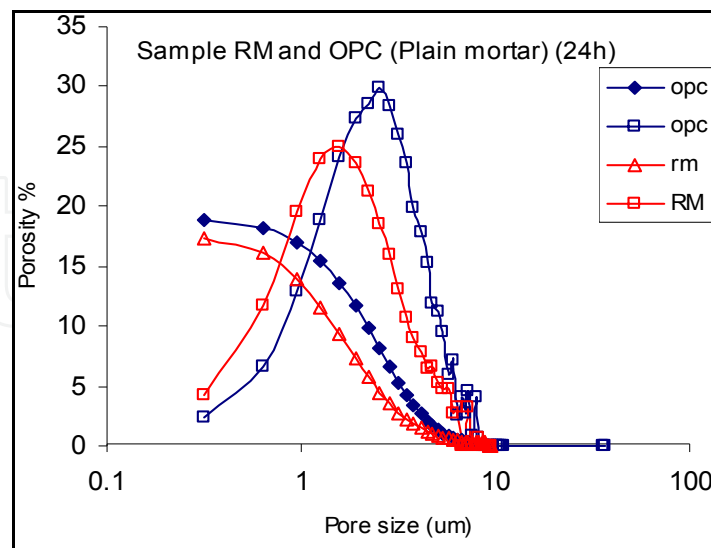
expected at 72 days (via the recorded OCP values, Fig. 8), the response with external polarization shows performance close to the control cases. In contrast, for the corroding specimens OPCn(NaCl) significantly higher corrosion and anodic currents are recorded at 72 days of stage (Fig. 9b). For the latest hereby reported interval (136 days), the corroding RMn(NaCl) specimen is already active (Fig. 9c), but still exhibiting lower anodic currents, compared to identically conditioned, corroding specimen OPCn(NaCl).

As evident from the electrochemical measurements, 20% red mud as cement replacement results in corrosion delay of approximately 5 times in the very aggressive environment of 10% NaCl. Similarly to BFS (as discussed in paragraph 2), the presence of RM in reinforced mortar (and concrete respectively) will account for an increased corrosion resistance in the wastes-modified systems. In order to clarify the responsible mechanisms and related phenomena, microstructural analysis of the bulk cementitious matrix is performed and discussed in what follows.



(a)

(b)



(c)

Fig. 10. Micrographs of the bulk cementitious matrix in OPC (a) and RM (b) plain mortar specimens after 24h hydration; porosity and pore size distribution for OPC and RM specimens at 24h hydration age (c)

3.2.2 Bulk matrix properties

Microstructural parameters (bulk matrix) were initially derived for plain (not-reinforced) mortar as a preliminary test (using identical to the reinforced mortar mixtures). Figure 10 depicts micrographs of the bulk matrix at 24h hydration age for a control OPC specimen (Fig. 10a) and control RM-containing specimen (Fig. 10b).

The recorded porosity and pore size distribution are shown in Fig. 10c). As seen from the plots, after 24h cement hydration the RM specimen presents slightly lower porosity (17.3%), compared to the OPC specimen (18.7%) and reduced pore size for the former, compared to the latter (compressive strength at 24h was also recorded as an average of three replicates per mortar type, resulting in similar values of 13 MPa at 24h). The above results are not entirely in line with the expectations i.e. since red mud is reported to have a pozzolanic activity it was expected that the difference in porosity will be more substantial. Further, a reduced porosity and pore size would account for reduced permeability of the cementitious matrix i.e. reduced chloride penetration would delay corrosion initiation. Therefore, porosity alone is not the only factor, causing microstructural alterations in the red mud containing cells, which apparently resulted in inhibition of corrosion. Further, porosity and pore size distribution were recorded for the bulk mortar matrix of the reinforced mortar specimens at 136 days. Figure 11 presents summarized bulk porosity values (a) and pore size distribution (b) for non-corroding (Ow and Rw) and corroding (On and Rn) mortar cells without (designation O) and with (designation R) red mud. It is obvious that 20% addition of red mud to the cement based matrix induces reduction of porosity, but not as pronounced as expected. The corroding cells from both types (Rn and On) would normally have lower porosity, compared to the relevant control specimens (Rw and Ow), since chloride is known to be a hydration accelerating factor and thus initially reduces porosity of the bulk matrix (Koleva D. A. 2007c). However, when chloride-induced corrosion is involved, the corrosion-induced cracking in the matrix (as consequence from formation and volume expansion of corrosion products at the steel/cement paste interface) contributes to the pore structure performance.

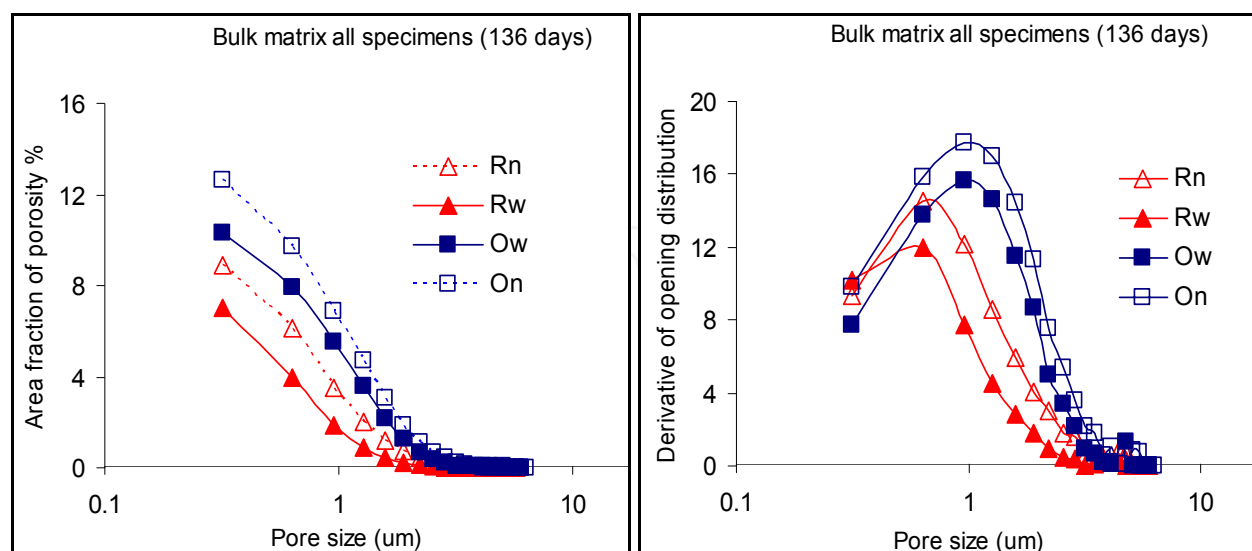


Fig. 11. Porosity (left) and pore size distribution (right) for reinforced mortar with and with and without red mud at 136 days of hydration age

Finally, if a comparison is made between all investigated specimens, the lowest porosity was recorded in the control specimens with red mud (Rw), almost equal to the corroding

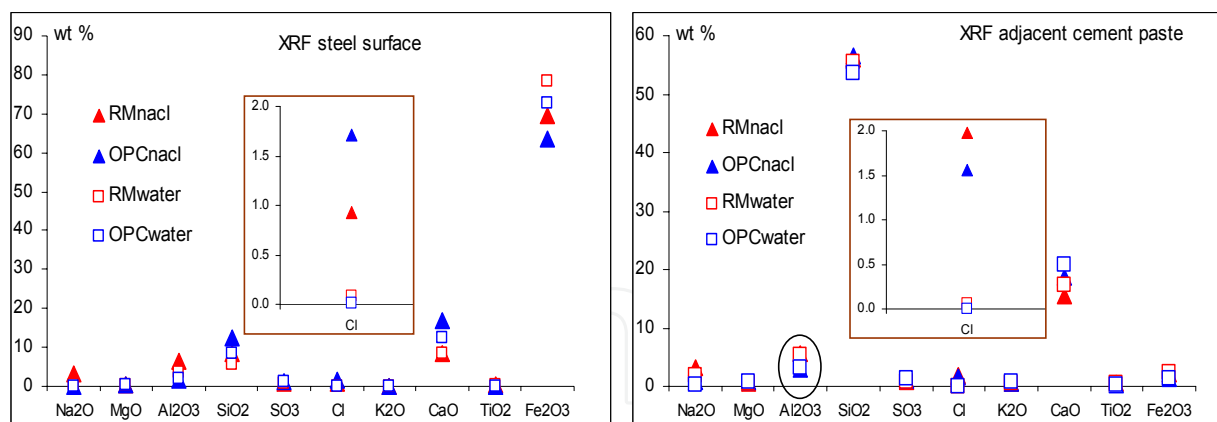


Fig. 12. XRF analysis of the product layers on the steel surface (left) and the adjacent cement paste (right) for all investigated specimens

specimen with red mud (Rn) i.e. red mud decreases bulk porosity in both cases. The highest recorded porosity (due to corrosion induced cracking) was in the corroding specimen without red mud (On), which was about 2% higher than the control one without red mud (Ow). Overall, it can be stated that the difference of 2.5 - 3% in porosity, relevant to all investigated conditions at 136 days of age, would not be the main and only factor, influencing to such a significant extent the corrosion resistance properties and behaviour.

The most plausible mechanism for the beneficial influence of red mud in terms of corrosion resistance is a combined effect of both red mud properties and microstructural changes: Red mud consists of a mixture of caustic insoluble minerals, originally present in bauxite, from which hematite (Fe_2O_3) has a major influence on the corrosion related phenomena (hematite is approximately 25% present in the used red mud) i.e. the presence of Fe^{3+} indicates a certain degree of redox activity (Ramanujan S. 1962, Skoulikidis T., et al.1992) on the steel surface and thus favours steel passivation. Furthermore, a possibly increased chloride binding mechanisms is relevant for the mixtures, containing red mud, as evidenced by XRF analysis on the steel surface and the adjacent cement paste (Fig. 12). As seen from the plots, the chloride concentration on the steel surface in corroding specimens RMNaCl is 1.5 times lower than the RM-free specimen OPCNaCl (Fig. 12, left), however, the chloride concentration in the cement paste, adjacent to the steel surface, is higher for the former (RMNaCl) and lower for the latter (OPCNaCl) case (Fig. 12, right).

Figure 13 presents light microscopy images of the steel surface (right column) and the immediately adjacent cement paste (left column) for OPC corroding (top row) and RM corroding (bottom row) specimens after 136 days of conditioning. Well visible is the significant corrosion damage (localised corrosion) in the RM-free specimen OPC. The corrosion products in the corroding specimens OPC volume expanded and deposited (penetrated) the adjacent cement paste (Fig. 13 top left). In contrast, for the RM corroding specimens, at the stage of 136 days only minor corrosion product accumulation was observed on the steel surface (Fig. 13); the corrosion products did not yet propagate and deposit in the adjacent cement paste (Fig. 13. bottom left). Considering also the ESEM microscopical investigation (again, directly on the steel surface and the adjacent cement paste (after 136 days) - Fig. 14), showing a well adhered product layer for control conditions in the presence of red mud (compare Fig. 14 a) and b)) and minimum or non corrosion products for the red mud-corroding cases (compare Figs. 14c) and d) and Fig. 13 b) and d)), it is obvious that several aspects are responsible for the positive effect of red mud on

corrosion resistance in reinforced concrete. In addition to slightly altered microstructural properties and apparently increased chloride thresholds, the properties of red mud are playing a role in the observed corrosion mechanisms.

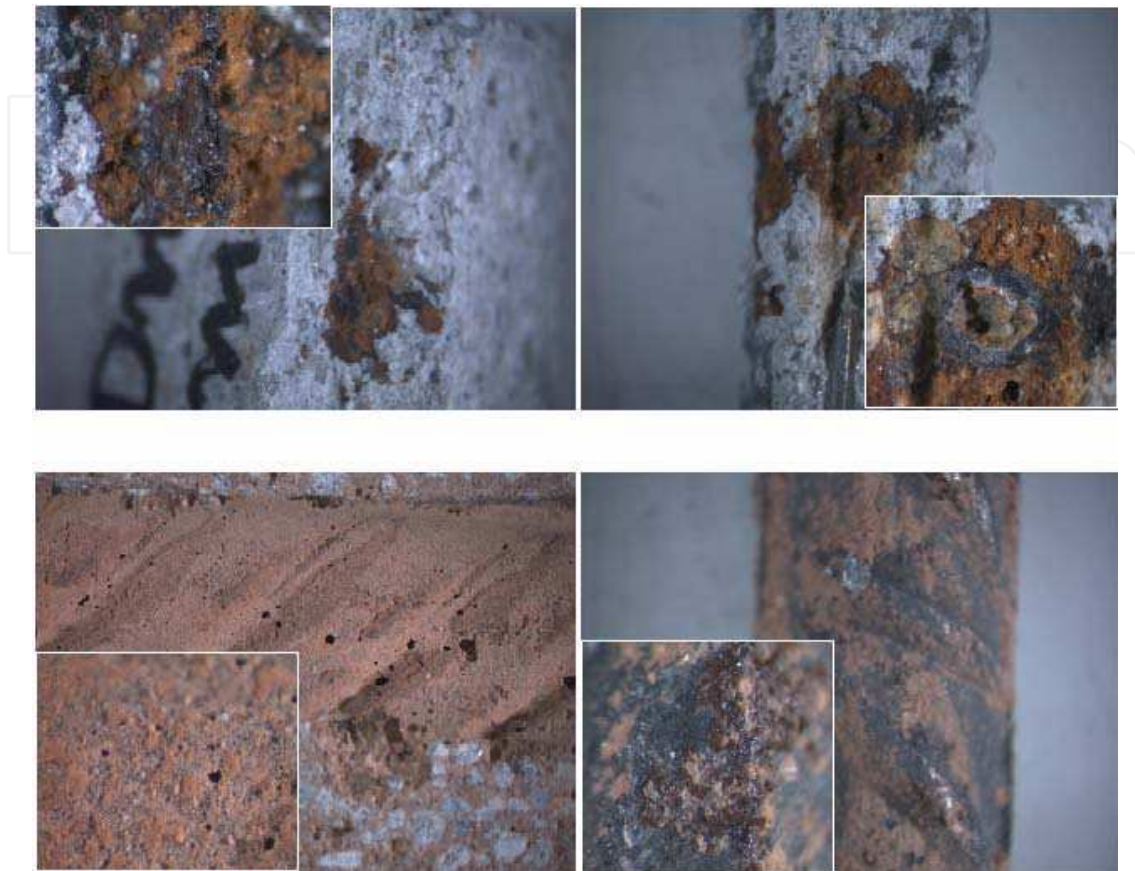


Fig. 13. Light microscopy of the cement paste, adjacent to the steel reinforcement (left) and steel surface (right) for corroding cells OPC (top row) and corroding cells RM (bottom row)

The surface charge of the RM particles is of significant importance for the chemical and physicochemical alterations in a cement-based matrix. As reported (Chvedov D., et al. 2001), there are ionized surface (OH⁻) groups on the RM particles' surface allowing them to perform as active sites and thus favouring their adhesion on a metallic surface (Díaz B., et al. 2004, Koleva D.A., et al. 2008d, Collazo A., et al. 2005). Thus, the steel surface in the red mud containing corroding specimens will have increased corrosion resistance due to a simple barrier effect of the adhered RM layer. Additionally, the surface groups can acquire protons without changing the pH of the surrounding medium i.e. reported are buffering effects of the RM particles (Chvedov D., et al. 2001, Stumm W. 1995, Atun G., et al. 2000). These latter effects will additionally delay corrosion initiation/corrosion propagation (as actually observed, no significant corrosion layer was formed on the steel surface (Figs. 13, 14d) or deposited in the adjacent cement matrix (Figs. 13, 14d) when red mud was admixed in reinforced mortar. Finally, the negatively charged RM particles can act as adsorption sites for Ca²⁺ or other positively charged ions, thus capture Cl⁻ (similar effect is also reported in (Collazo A., et al. 2005) as evident from XRF analysis (Fig. 12). Summarizing, this paragraph briefly discussed an eco-friendly approach to corrosion control via waste utilization, in particular a largely generated waste from the aluminum production (red mud). Reinforced

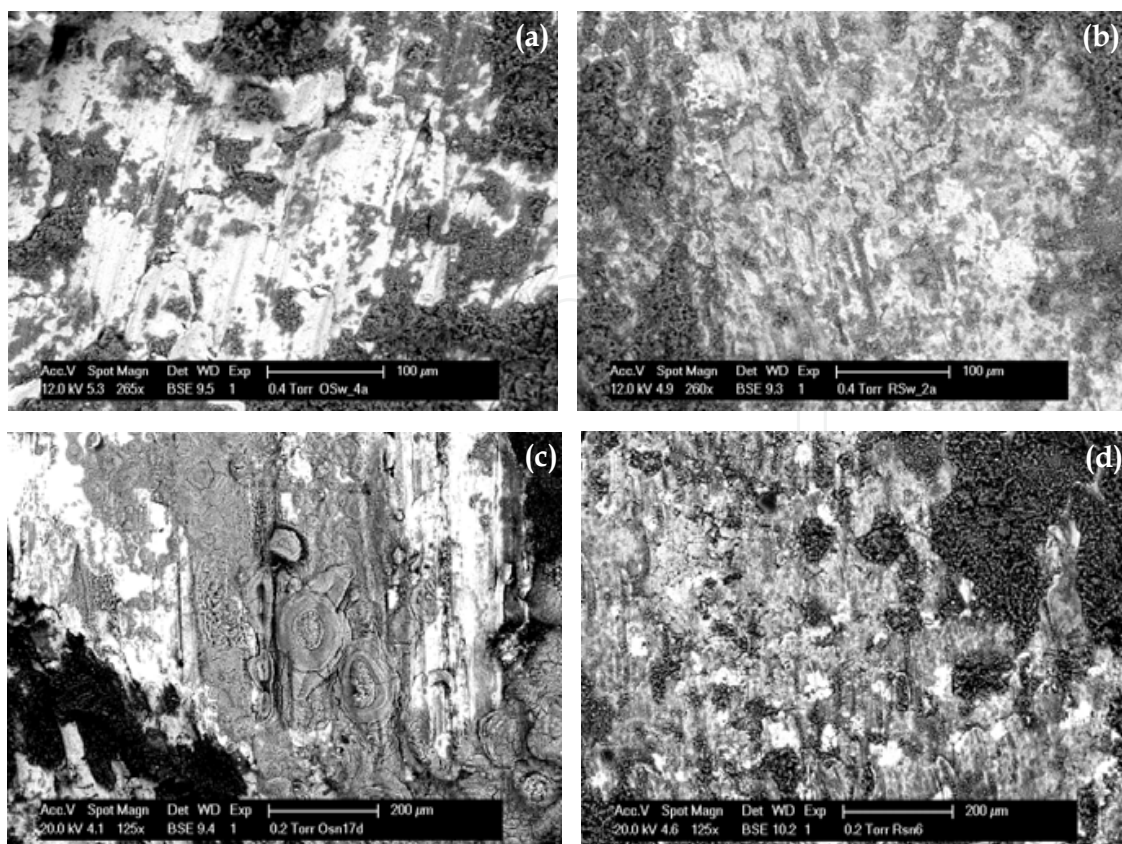


Fig. 14. ESEM micrographs for the steel surface (and product layers respectively) for control OPC and RM cells (a,b) and corroding OPC and RM cell (b,d)

mortar, using 20% cement replacement with red mud was evaluated in terms of steel corrosion behaviour and bulk matrix properties. The electrochemical monitoring (7 until 136 days) proves the higher corrosion resistance of Red Mud containing reinforced mortar in highly aggressive environment (10 % NaCl) i.e. 20% red mud (as cement replacement) leads to approximately 5 times delay in corrosion initiation (compared to red mud - free mixtures). Slightly lower porosity and pore size distribution was recorded for the bulk matrix of the red mud - containing mortar (without calcination of the red mud before admixing). The positive effect of red mud lies in the combined influence on microstructural properties, redox activity and thus favouring steel passivation and the peculiarities (as surface charge) of the red mud particles themselves. Similarly to BFS cement mortar/concrete (paragraph 2) this paragraph illustrated the importance of an integrated approach (electrochemistry and concrete material science) for a thorough investigation of a reinforced cement-based system and for clarifying the phenomena, responsible for the observed behaviour in the relevant conditions.

4. Conclusions

This chapter discussed and gave examples for the integration of electrochemical methods and microstructural investigation in reinforced cement-based materials within conditions of chloride-induced corrosion. An eco-friendly approach to corrosion control in reinforced cement-based systems, by involving waste utilization (slag, from the steel production and red mud, from the aluminum production) was also discussed, presenting material properties and materials interactions in the context of increased corrosion resistance.

For the hereby reported period of 28 to 150 days for reinforced concrete and 7 until 136 days for reinforced mortar, the specimens cast with OPC CEM I only exhibit active corrosion behaviour and reduced corrosion resistance, whereas passive state or minimal corrosion activity was recorded for the identically conditioned BFS (CEMIII) and RM (cement replacement with red mud) specimens.

For reinforced concrete (paragraph 2), in the BFS specimens corrosion at the stage of 150 days was still not initiated (corrosion medium of 5% NaCl) and they behave as "passive" (control) cells. The beneficial effect of BFS in terms of delay in corrosion initiation, is obvious: significantly higher corrosion resistance (impedance $|Z|$ and derived R_{ct} values respectively), no chlorides accumulated in the immediate vicinity of the steel surface, increased concrete resistivity. Apparently, the bulk cement matrix in the BFS specimens plays a significant role in the observed behaviour. Additionally, the electrochemical parameters for the embedded steel were correlated with the microstructural parameters and properties of the bulk concrete matrix. The higher corrosion resistance in BFS concrete is not related to the postulated lower porosity, or higher chloride binding capacity, but is denoted to significantly lower pore network capacitance and higher pore network resistance i.e. decreased pore-network interconnectivity and permeability, verified with microstructural analysis. In that sense EIS is proved to be a valuable tool for non-destructive and thorough evaluation of a reinforced concrete system.

For the series of reinforced mortar (paragraph 3) open circuit potential mapping of the embedded steel (corrosion medium of 10% NaCl) shows that 20% red mud as cement replacement in the mortar mixture, significantly delays corrosion initiation i.e. in the specimens containing red mud, corrosion starts after 70 to 85 days, while in the "control" (corroding) samples corrosion was initiated 10 to 15 days after immersion in NaCl. Polarization resistance values clearly show the increased corrosion resistance of the red mud containing corroding cells and the above stated delay in corrosion initiation. The addition of red mud slightly decreases porosity and critical pore size in the bulk cementitious matrix through increasing the chloride binding capacity of the latter, evidenced by the lack of free chlorides at the steel/paste interface in the specimens, containing red mud. Furthermore, the negatively charged red mud particles most likely act as adsorption sites for positively charged species (Ca^{2+} , Al-hydrates etc.) and thus result in "capturing" chloride ions. Further investigation is clearly necessary to provide firm evidence for the surface charge, absorption mechanisms and the positive influence of red mud particles in terms of favored passivation and/or buffering effects on the steel surface in reinforced cement-based materials.

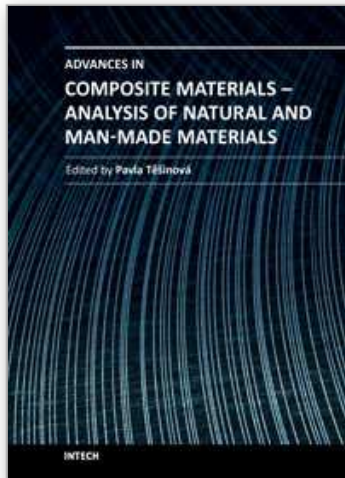
In conclusion, EIS is a powerful and valuable tool for characterizing a reinforced concrete system, in terms of corrosion performance of the steel surface, but providing information for the properties of the bulk cement-based matrix as well. Thus, fundamental electrochemistry (in the sense of widely known and applied electrochemical techniques) is an essential part of studies related to reinforced concrete (and therefore applicable in the field of civil engineering). The proper evaluation of a reinforced concrete system is only possible via the application of electrochemical techniques and a thorough characterization of the involved phenomena can be achieved via the integrated approach of electrochemical science and concrete material science.

5. References

- Amritphale S.S, Anshul A, Chandra N, Ramakrishnan N, (2007) A novel process for making radiopaque materials using bauxite – Red mud, *Journal of the European Ceramic Society* 27, 1945–1951

- Atun G., Hisarli G., (2000) *J. Colloid Interf. Sci.* 228, 131.
- Audenaert K., Yuan Q., De Schutter G., (2010) *Constr. Build. Mater.* 24, 396.
- Ayres R.U, John H. and Bjorn A, (2001) Utilisation of wastes in the new millennium. *MRSI Bull.*, 7, 477-480
- Baweja D., Roper H., Sirivivatnanon V., (1998) *ACI Mater. J.* 207.
- Bouikni A., Swamy R.N., Bali A., (2009) *Constr. Build. Mater.* 23, 2836.
- Cengeloglu Y, Tor A , Arslan G, Ersoz M, Gezgin S, (2007) Removal of boron from aqueous solution by using neutralized red mud, *Journal of Hazardous Materials*, 142, 1-2, 412-417
- Chvedov D., Ostap S., Le T., (2001) *Colloids Surf. A* 182, 131.
- Collazo A., Fernandez D., Izquierdo M., Novoa X.R., Perez C., (2005) *Progress in Organic Coatings*, 52, 351-358.
- Collazo A., Izquierdo M., Novoa X.R., Perez C., (2007) Surface treatment of carbon steel substrates to prevent cathodic delamination, *El. Acta* 52, 7513-7518.
- Copuroglu O., (2006a) *PhD Thesis, Frost salt scaling of cement-based materials with a high slag content. TUD Technische Universiteit Delft.*
- Çopuroğlu O., Fraaij A.L.A., Bijen J.M.J.M., (2006b) *Cem. Concr. Res.* 36, 1475.
- Dehghanian C., Arjemandi M., (1997) *Cem. Concr. Res.* 27, 937.
- Dehghanian C., (1999) *Corrosion* 55, 291.
- Dhoubi L., Triki E., Raharinaivo A., (2002) *Cem. Concr. Comp.* 24, 35.
- Díaz B., Joiret S., Keddam M., Nóvoa X. R., Pérez M. C., Takenouti H., (2004) Passivity of iron in red mud's water solutions, *Electrochimica Acta*, 49, 3039-3048.
- Díaz B., Nóvoa X.R., Pérez M.C., (2006) *Cem. Concr. Comp.* 28, 237.
- Dinakar P., Babu K.G., Santhanam M., (2007) *Cem. Concr. Comp.* 29, 136
- Efes Y., (1980) *in: Betonwerk und Fertigtiel Technik (Wiesbaden)* 46 (4) 224-229.
- Fedrizzi L., Azzolini F., Bonora P. L., (2005) *Cem. Concr. Res.* 35, 551.
- Feliú V., González J. A., Andrade C., Feliú S., (1998) *Corr. Sci.* 40, 975.
- Feliú V., González J. A. and Feliú S., (2004) *J. Electrochem. Soc.* 151, B134.
- Giorv O. E., Vennesland O., (1979) *Cem. Concr. Res.*, 9, 229.
- Gjorv O. E., (1995) *ACI Mater. J.* 92, 591.
- Glass G.K., Buenfeld N.R., (1997) *Corros. Sci.*, 39, 1001.
- Gu P., Beaudoin J.J., Zhang M.H., Malhotra V.M., (2000) *ACI Mater. J.* 97, 254.
- Hooton R.D., (1986) *In: Frohnsdorff G, ed. Blended cement, ASTM STP 897; 128.*
- Hossain K. M. A., Lachemi M., (2004) *Cem. Concr. Res.* 34, 695.
- Hu J., Stroeven P., (2003) *Image Analysis Stereology*, 22, 97.
- Irassar E. F., Gonzalez M., Rahhal V., (2000) *Cem. Concr. Compos.* 22, 361.
- Koleva D.A., de Wit J.H.W., van Breugel K., van Westing E., (2007a) *J. Electrochem. Soc.* 154, P52.
- Koleva D.A., Hu J., Fraaij A., van Breugel K., de Wit J.H.W., (2007b) *Cem. Concr. Res.*, 37, 604.
- Koleva D. A., (2007c) *Corrosion and Cathodic Protection in Reinforced concrete, PhD Thesis, Delft University of Technology, Delft.*
- Koleva D.A., Copuroglu O., van Breugel K., Ye G., de Wit J.H.W., (2008a) Electrical resistivity and microstructural properties of concrete materials in conditions of current flow, *Cem.Concr.Compos.*, 30, pp 731-744
- Koleva D. A., de Wit J.H.W., van Breugel K., Veleva L.P., van Westing E., Copuroglu O., Fraaij A.L.A., (2008b) *Mater. Character.* 59, 801.
- Koleva D. A., van Breugel K., de Wit J.H.W., van Westing E., Copuroglu O., Veleva L., Fraaij A.L.A., (2008c) *Mater. Character.* 59, 290.
- Koleva D.A., Copuroglu O., van Breugel K., de Wit J.H.W., (2008d) "EIS and PDP of construction steel in cement extract, containing red mud and chloride

- contamination", 214th Joint Meeting of the Electrochemical Society and the Electrochemical Society of Japan, Honolulu, Hawaii, US, 11th - 17th October 2008, www.electrochem.org
- Koleva D. A., Guo Z., van Breugel K., de Wit J. H. W., (2009) *Mater. Corrosion* 60, 344.
- Koleva D.A., (2010a) Corrosion resistance of construction steel in BFS and OPC concrete: correlation of electrochemical parameters and microstructural characteristics, *Corr.Sci.* submitted
- Koleva D. A., Guo Z., van Breugel K., de Wit J. H. W., (2010b) *Mater. & Corrosion*, *In press*, DOI: 10.1002/maco.200905423
- Koleva D.A., (2011), The significant delay of a chloride-induced corrosion in reinforced mortar, containing red mud as cement replacement, Submitted to J. Electrochem. Soc.
- Kumar A.D.M. (1986), *In: Proc. 8th Conf. Chemistry of Cement, Brazil*, 73.
- Li L.Y, (1998) *Environmental Engineering* 3, 254.
- Li S., Roy Della M., (1986) *Cem. Concr. Res.*16, 749.
- Macphee D.E., Cao H.T., (1993) *Mag. Concr. Res.* 45, 63.
- Manmohan D., Mehta P.K., (1981) *Cem. Concr. Aggr.* 3, 63.
- Montemor M. F., Cunha M. P., Ferreira M. G., Simões A. M., (2002) *Cem. Concr. Comp.* 24, 45.
- Mymrin V., de Araujo P., Lopes H., Ferreira O., (2003) Environment friendly method of high alkaline bauxite's red mud and ferrous slag utilization as an example of green chemistry, *Green Chem.*, 5, 357-360
- Osborne G.J., (1999) *Cem. Concr. Compos.* 21, 11.
- Page C. L., (2002) *in: Proc. 15th Intern. Corrosion Congress, Granada*
- Pal S.C., Mukherjee A., Pathak S.R., (2002) *ACI Mater. J.* 99, 1.
- Petterson K., (1994) *in: Corrosion and corrosion protection of steel in concrete*, Ed. Swamy RN, Academic Press, Sheffield, 461.
- Ramanujan S., (1962) *Paintindia* 12, 22.
- Ramezani pour A.A., (1995) *Cem. Concr. Compos.* 17, 125.
- Sagüés A. A., Kranc S. C., Moreno E.I., (1995) *Corr. Sci.* 37, 1097.
- Serra J., (1982) *Image analysis and mathematical morphology*. London: Academic Press.
- Skoulikidis T., Vassiliou P., Diamantis N., Tunturi P.J. (1992) (Eds.), *Proc. of 12th Scand. Corros. Congr. Eurocorr'92*, Corros. Soc. of Finland, p. 475.
- Song Ha-Won, Saraswathy V., (2006) *J. of Hazardous Materials* B138 226.
- Stumm W., (1995) *Chemistry of the Solid-Water Interface*, Wiley, New York, (Chapters 2-6).
- Suryavanshi A.K., Scantlebury J.D., Lyon S.B., (1995) *Cem. Concr. Res.* 25, 980.
- Thomas M. D. A., Bamforth P.B., (1999) *Cem. Concr. Res.* 29, 487.
- Tsakiridis P.E., Agatzini-Leonardou S., Oustadakis P., (2004) Red mud addition in the raw meal for the production of Portland cement clinker *Journal of Hazardous Materials*, 116, 1-2, 103-110.
- Vassie P.R.W., (1984) *Proc. Inst. Civ. Engrs.*, 76, 713.
- Wenger F., Galland J., (1990) *Electrochim. Acta* 35, 1573.
- Ye G., (2003) *Experimental Study and Numerical Simulation of the Development of the Microstructure and Permeability of Cementitious Materials*, PhD thesis, Delft University of Technology, Delft.
- Yong Liu, Chuxia Lin, Yonggui Wu., (2007) Characterization of red mud derived from a combined Bayer Process and bauxite calcination method, *J. of Hazardous Materials*, 146, 255-261



Advances in Composite Materials - Analysis of Natural and Man-Made Materials

Edited by Dr. Pavla Tesinova

ISBN 978-953-307-449-8

Hard cover, 572 pages

Publisher InTech

Published online 09, September, 2011

Published in print edition September, 2011

Composites are made up of constituent materials with high engineering potential. This potential is wide as wide is the variation of materials and structure constructions when new updates are invented every day. Technological advances in composite field are included in the equipment surrounding us daily; our lives are becoming safer, hand in hand with economical and ecological advantages. This book collects original studies concerning composite materials, their properties and testing from various points of view. Chapters are divided into groups according to their main aim. Material properties are described in innovative way either for standard components as glass, epoxy, carbon, etc. or biomaterials and natural sources materials as ramie, bone, wood, etc. Manufacturing processes are represented by moulding methods; lamination process includes monitoring during process. Innovative testing procedures are described in electrochemistry, pulse velocity, fracture toughness in macro-micro mechanical behaviour and more.

How to reference

In order to correctly reference this scholarly work, feel free to copy and paste the following:

D. A. Koleva and K. van Breugel (2011). The Synergy of Electrochemistry and Concrete Material Science in Evaluating Corrosion Resistance of Wastes-Containing Reinforced Cement-Based Systems, *Advances in Composite Materials - Analysis of Natural and Man-Made Materials*, Dr. Pavla Tesinova (Ed.), ISBN: 978-953-307-449-8, InTech, Available from: <http://www.intechopen.com/books/advances-in-composite-materials-analysis-of-natural-and-man-made-materials/the-synergy-of-electrochemistry-and-concrete-material-science-in-evaluating-corrosion-resistance-of->

INTECH
open science | open minds

InTech Europe

University Campus STeP Ri
Slavka Krautzeka 83/A
51000 Rijeka, Croatia
Phone: +385 (51) 770 447
Fax: +385 (51) 686 166
www.intechopen.com

InTech China

Unit 405, Office Block, Hotel Equatorial Shanghai
No.65, Yan An Road (West), Shanghai, 200040, China
中国上海市延安西路65号上海国际贵都大饭店办公楼405单元
Phone: +86-21-62489820
Fax: +86-21-62489821

© 2011 The Author(s). Licensee IntechOpen. This chapter is distributed under the terms of the [Creative Commons Attribution-NonCommercial-ShareAlike-3.0 License](#), which permits use, distribution and reproduction for non-commercial purposes, provided the original is properly cited and derivative works building on this content are distributed under the same license.

IntechOpen

IntechOpen